Mon. Not. R. astr. Soc. (1988) **235**, 633–653

The chemical composition gradient across M 33

J. M. Vílchez[1], B. E. J. Pagel[2], Angeles I. Díaz[3], Elena Terlevich[4]* and M. G. Edmunds[5]

[1]*Instituto de Astrofísica de Canarias, 38200-La Laguna, Tenerife, Spain*
[2]*Royal Greenwich Observatory, Herstmonceux BN27 1RP*
[3]*Dpto. de Física Teórica, C-XI, Universidad Autónoma de Madrid, 28049-Madrid, Spain*
[4]*Astronomy Centre, Sussex University, Falmer, Brighton BN1 9QH*
[5]*University College, P.O. Box 78, Cardiff CF1 1XL*

Accepted 1988 May 26. Received 1988 May 25; in original form 1988 March 11

Summary. The abundance gradient in M 33 is studied on the basis of IPCS and CCD data on emission lines in selected H II regions, using O II, O III, S II and S III in the wavelength range $\lambda\lambda$3700–9600 Å to refine the oxygen abundances in the inner parts as well as to study the behaviour of S/O.

Spatially resolved observations in each H II region permit the ionization structure to be studied and enable ionization parameters and stellar effective temperatures to be separately determined. The main results are (i) the hardness of the ionizing radiation and the ionization parameter increase outwards (with diminishing abundances) along the galactic radius; (ii) the O/H gradient is steep in the inner regions, but much flatter in the outer regions; (iii) N/O is constant over most of the visible disc, but lower in an outer H II region; and (iv) the S/H gradient is shallower than the O/H gradient exemplifying what appears to be a universal trend for S/O to decrease with O/H in H II regions. This latter trend is rather unexpected from the viewpoint of nucleosynthesis theory.

1 Introduction

Spectroscopic observations of giant extragalactic H II regions (GEHR) are an essential tool for the determination of element abundances in the interstellar medium of external galaxies and knowledge of these abundances and their variations is of the greatest importance for the study of the chemical evolution of galaxies. A considerable amount of work has been developed on this topic during the last decade (see review by Pagel & Edmunds 1981 and references therein; McCall, Rybski & Shields 1985; Terlevich *et al.*, in preparation). However, in spite of many achievements on the observational side there are still some outstanding problems in the interpretation of the spectra, particularly those of low and moderate excitation GEHR in the discs of

*Present address: Royal Greenwich Observatory, Herstmonceux BN27 1RP.

spirals for which the electron temperature cannot be directly measured from auroral lines. This problem has been treated in different ways:

(i) the use of radio lines to determine electron temperatures (Shaver *et al.* 1983);

(ii) the empirical approach of Pagel *et al.* (1979) and Alloin *et al.* (1979) to determine abundances and/or electron temperatures from selected nebular line ratios;

(iii) the modelling approach which has been applied in two different ways: individual modelling (Shields & Searle 1978; Evans & Dopita 1985; Evans 1986; Shields 1986; Dinerstein & Shields 1986; Garnett & Shields 1987); and model sequences (McCall *et al.* 1985; Dopita & Evans 1986).

The first method cannot be used for most H II regions in external galaxies due to the lack of radio sensitivity and spatial resolution. Regarding the other two methods, if the required spectral information is available, individual models are always preferred, as a rule, to the prediction of the sequential calibrations which have the weakness of needing at least two parameters: initial mass function and age. Nevertheless, it seems that an estimation of the abundance (within a factor of two) can be obtained from the revised empirical calibration of Edmunds & Pagel (1984) as presented by Dopita & Evans (1986).

There is yet another independent approach to determine the abundance and some physical properties of the GEHR which consists in the simultaneous fitting of the empirical parameters for the abundance (Edmunds & Pagel 1984) and the ionizing spectrum (Vílchez & Pagel 1988). This approach allows a definitive selection of the appropriate model from a grid, and it seems to work successfully for a sample including some classically problematic GEHR (Vílchez 1987).

In any case, the interpretation of GEHR spectra in terms of abundance, while straightforward for high excitation objects, requires a wide spectroscopic coverage and high quality observations for low and moderate excitation GEHR, even when detailed modelling is available. Spatially resolved observations add the extra advantage of allowing a direct confrontation of model predictions with observations over a variety of excitation conditions.

In 1984 we started a programme to perform long-slit spectroscopic observations of GEHR in nearby galaxies over a wide range in wavelength (λ3700 Å–1 μm) that would allow reliable abundance determinations of regions as close as possible to their centres. The galaxy M 33 offers a great opportunity to study the chemical composition and ionization structure of GEHR since it is nearby; there are many extended H II regions (Boulesteix *et al.* 1974; Courtès *et al.* 1987); and the inclination is not excessive. Although there exist previous studies in the optical range for some H II regions (Smith 1975; Kwitter & Aller 1981) and supernova remnants (Dopita, D'Odorico & Benvenuti 1980; Blair & Kirshner 1985), different sources are not entirely consistent.

In previous work (Díaz *et al.* 1987, Paper I) we performed a detailed spectroscopic study of NGC 604 in the outer part of M 33, where we derived abundances from high quality data for selected regions within the complex, in order to investigate the chemical homogeneity over a scale of hundreds of parsecs. No significant variations in total chemical abundances were found despite the presence of WR stars and a SN remnant. In this paper we present spectroscopic observations for a set of six more selected H II regions spaced in radius along the disc of M 33 from the inner parts, near the nucleus itself, up to the outer zone of the galaxy. The proximity of M 33, and the instrumental configuration used, allowed us to obtain high signal-to-noise spatially resolved spectroscopy in reasonable exposure times. It is necessary to stress the importance of the near infrared observations since they provide an opportunity to check the abundance calibration and study the sulphur abundance gradient simultaneously with those of oxygen and nitrogen, thus reinforcing confidence in the abundance analysis. The wide spectral and spatial coverage, within an H II region and over the galaxy, offers enough information to effectively constrain models and empirical calibrations by studying the ionization structure.

In the following section we describe the observations; Section 3 presents results which are discussed in Section 4; our main conclusions are summarized in Section 5.

2 Observations and data reduction

The observations were obtained during two periods in 1984, from August 18–25 and December 19–22, using the RGO long-slit spectrograph at the cassegrain focus of the Isaac Newton Telescope at the Observatorio del Roque de los Muchachos (La Palma). A total of seven M 33 GEHRs, including NGC 604, were observed combining two detectors IPCS and CCD with the 235 mm camera, in order to cover a wide range in wavelength from λ3600 Å to 1 μm. Plate 1 shows the selected regions over an Hα photograph of M 33. A detailed description of the instrumental configuration used was presented in Paper I. We obtained high (0.5 Å pixel^{-1}) and intermediate (2 Å pixel^{-1}) dispersion IPCS spectra, and intermediate CCD ones (2 Å pixel^{-1}). The spatial resolution is 1″.5 and 0″.7 per pixel for the IPCS and CCD spectra respectively.

The high dispersion spectra covering from λ4250 to 5250 Å were intended to obtain measurements, or stringent upper limits, for the flux in the line [O III] λ4363 Å. This line was detected in the highest signal-to-noise (S/N) spectra which, in some cases, also show clearly the presence of stellar features associated with WR stars (see Paper I). A journal of the observations is presented in Table 1, excluding NGC 604 which was presented in Paper I. The data reduction was performed at the RGO STARLINK node using standard routines as described in Paper I.

For the abundance analysis we have used one integrated spectrum for each H II region or H II complex, obtained by compressing selected sets of spatial increments based on the Hα spatial profiles shown in Fig. 1. In suitable cases, point by point analysis was performed for the study of the ionization structure.

Table 1. Journal of observations.

Region	Night	Detector	P.A.	Grating	$\Delta\lambda$(Å)	Exposure (s)
IC 142	84 Aug. 19/20	CCD	352°	400*R*	6300–7600	500
IC 142	84 Aug. 19/20	CCD	352°	400*R*	8500–9800	1000
IC 142	84 Aug. 22/23	IPCS	352°	300*V*	3500–7400	1003
MA 2	84 Aug. 20/21	CCD	0°	400*R*	6300–7600	1000
MA 2	84 Aug. 20/21	CCD	0°	400*R*	7400–8700	1000
MA 2	84 Aug. 20/21	CCD	0°	400*R*	8500–9800	1500
MA 2	84 Aug. 22/23	IPCS	0°	300*V*	3500–7400	2059
CC 93	84 Aug. 20/21	CCD	0°	400*R*	6300–7600	1000
CC 93	84 Aug. 20/21	CCD	0°	400*R*	8500–9800	2000
IC 131	84 Aug. 22/23	IPCS	352°	300*V*	3500–7400	1806
IC 131	84 Aug. 22/23	IPCS	352°	300*V*	3500–7400	2000
IC 131	84 Aug. 23/24	IPCS	352°	1200*B*	4260–5260	3000
IC 131	84 Aug. 23/24	IPCS	352°	1200*B*	4260–5260	3500
NGC 588	84 Aug. 22/23	IPCS	352°	300*V*	3500–7400	1505
NGC 588	84 Aug. 23/24	IPCS	352°	1200*B*	4260–5260	3070
NGC 588	84 Aug. 23/24	IPCS	352°	1200*B*	4260–5260	1500
NGC 588	84 Dec. 20/21	CCD	320°	400*R*	4260–5260	3070
NGC 588	84 Dec. 20/21	CCD	320°	400*R*	8500–9800	3500
NGC 595	84 Aug. 24/25	IPCS	0°	1200*B*	4260–5260	1500
NGC 595	84 Aug. 24/25	IPCS	290°	1200*B*	4260–5260	3000
NGC 595	84 Aug. 24/25	IPCS	290°	1200*B*	4260–5260	1500
NGC 595	84 Dec. 19/20	CCD	0°	400*R*	6300–7600	2000
NGC 595	84 Dec. 19/20	CCD	0°	400*R*	7400–8700	2000
NGC 595	84 Dec. 19/20	CCD	0°	400*R*	8500–9800	3500

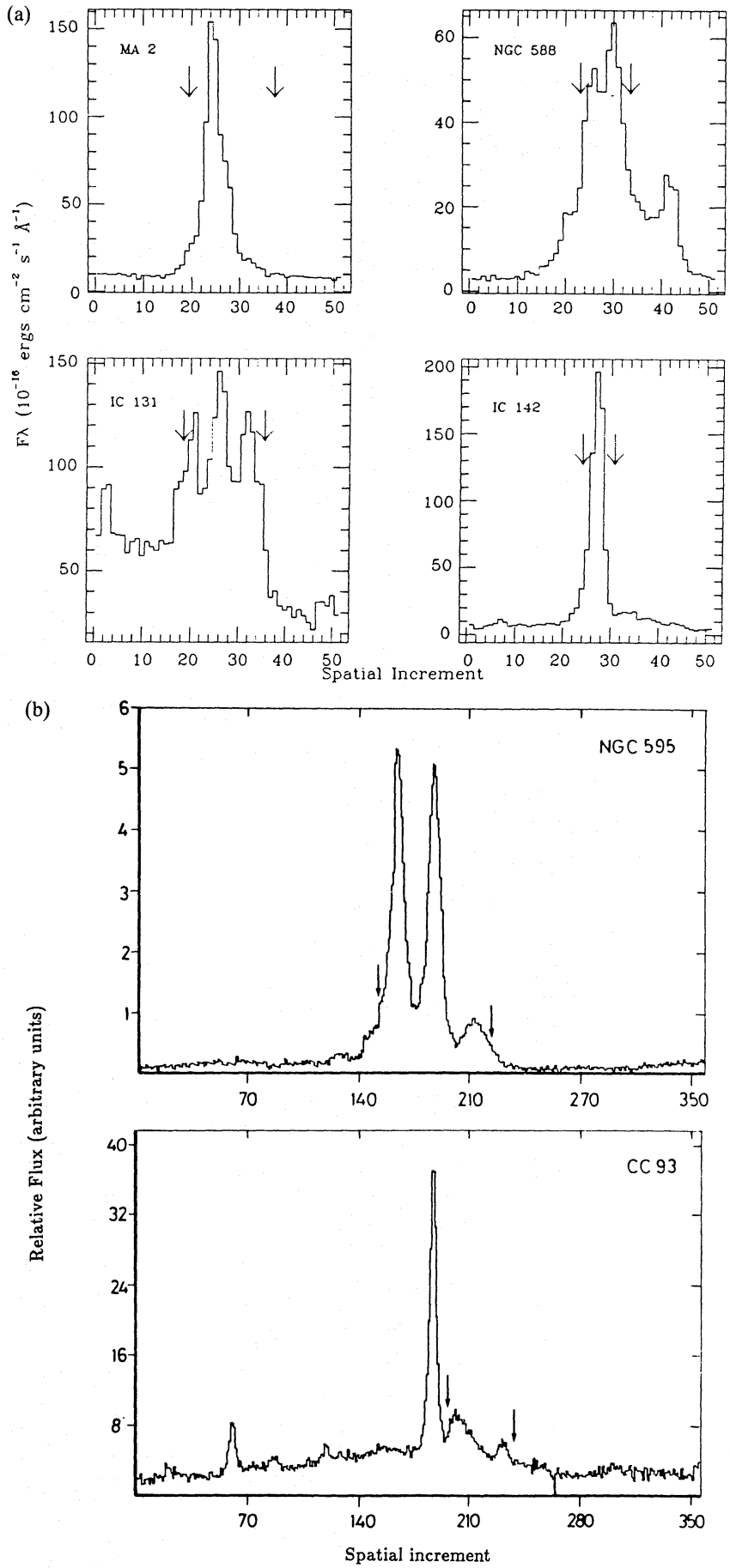

Figure 1. Spatial profiles of Hα for the HII regions of the sample extracted from (a) IPCS observations (MA 2, NGC 588, IC 131 and IC 142) and (b) CCD observations (NGC 595 and CC 93). The arrows mark the regions selected along the slit. The brightest part in the profile of CC 93 corresponds to the nucleus of M 33.

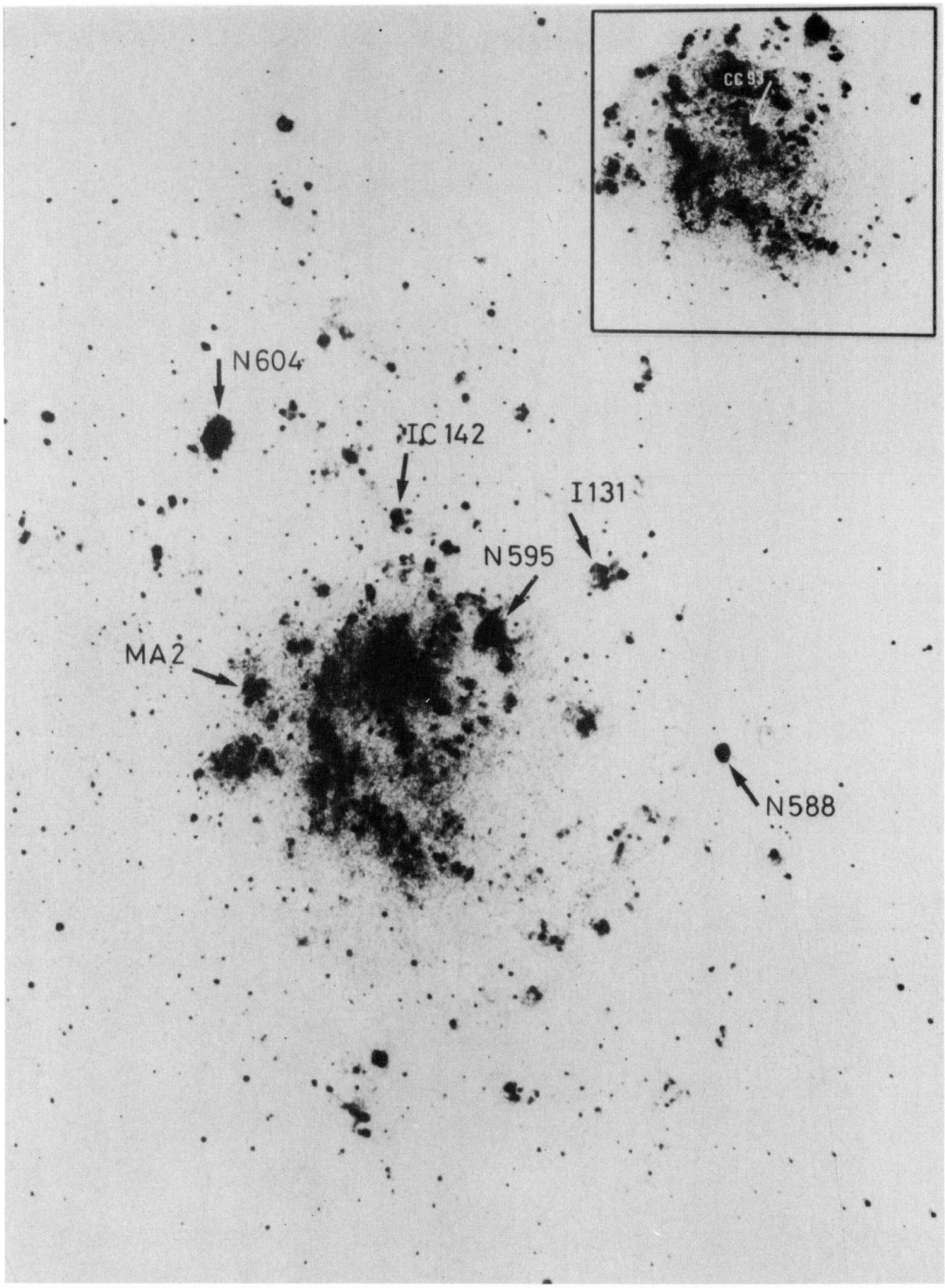

Plate 1. The H II regions selected for this study are indicated on this Hα photograph of M 33 taken from Boulesteix *et al.* (1974). The nuclear zone is shown (inset) to indicate the position of CC 93, the most inner region of our sample. Scale 3.2 mm/arcmin^{-1}.

The wavelength calibration was accurate to 1 Å in all cases. The sky subtraction process was very efficient judging from the absence of any residual atmospheric emission at the wavelength of the prominent sky lines. The red CCD spectra are further affected by atmospheric absorption, requiring a more elaborate process to correct for this effect (see Paper I). The line [S III] λ9532 Å is the one most affected by absorption and therefore we have decided not to use it for our analysis since it bears a fixed ratio to λ9069 Å.

For every region observed we have obtained IPCS and CCD spectra with two exceptions: for CC 93, the innermost region, we have only taken CCD spectra and for IC 131 only IPCS ones. For NGC 595, the optical information is restricted to the high dispersion spectra centred on λ4700 Å.

3 Results

3.1 LINE INTENSITIES

Fig. 2 shows some representative high (IPCS) and intermediate (IPCS and CCD) resolution spectra. The relative importance of the underlying stellar population is evidenced by the prominent bands at $\lambda\lambda$4600,5800 Å due to WN and WC stars (see D'Odorico, Rosa & Wampler 1983; Massey & Conti 1983 and Paper I) shown in Fig. 3. This spectrum corresponds to a localized region of IC 131 extracted from the larger area used for our abundance analysis.

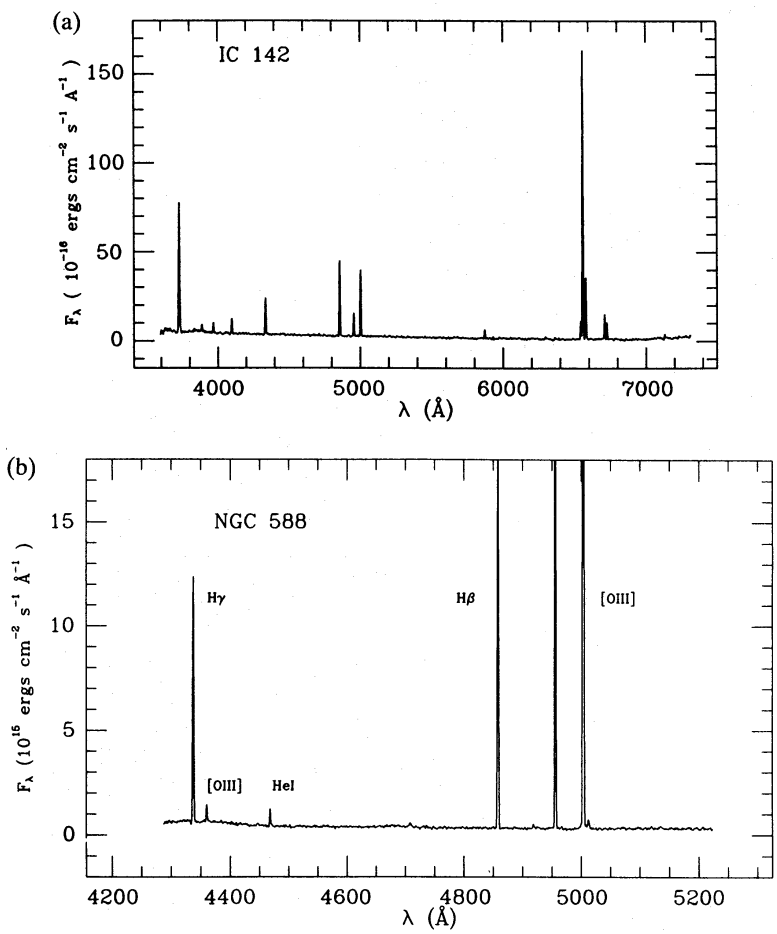

Figure 2. Representative spectra: (a) Intermediate dispersion IPCS spectrum of IC 142. Absence of emission or absorption features at the wavelengths of the most prominent sky lines ($\lambda\lambda$5577, 6300 Å) indicates the quality of the sky subtraction procedure. (b) High dispersion IPCS spectrum of NGC 588. The weak emission lines of [O III] λ4363 Å and He I λ4471 Å are clearly visible. (c) Intermediate dispersion CCD spectrum of NGC 595.

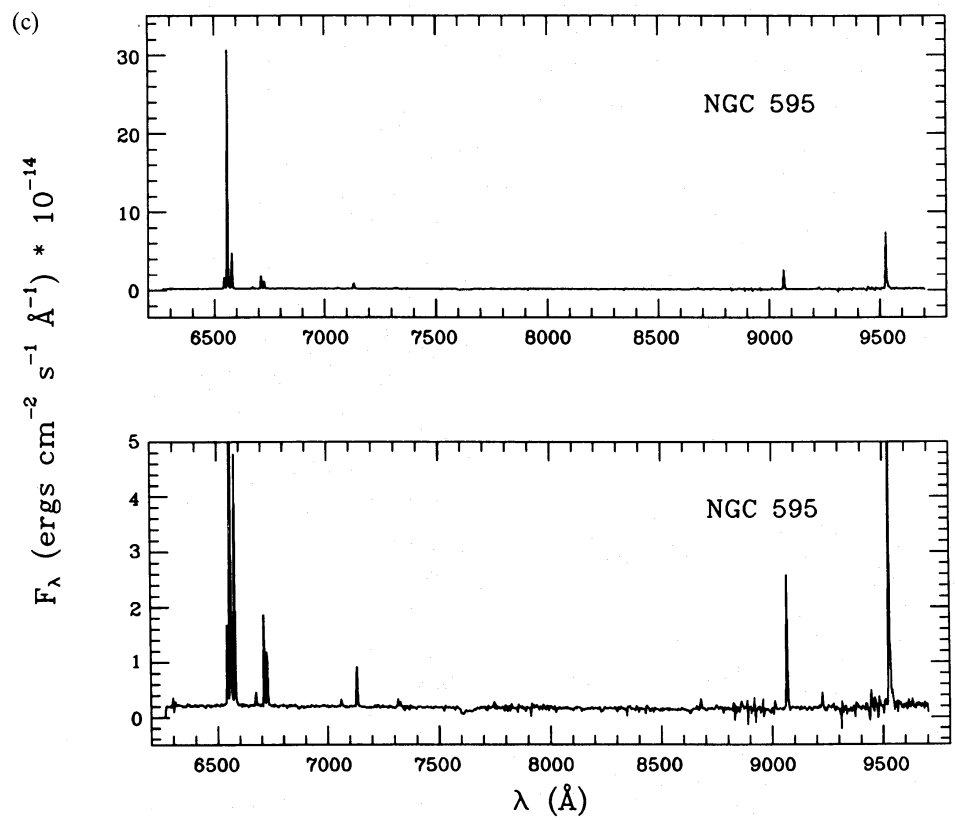

Figure 2–*continued*

Emission line fluxes were measured using the program LINES, kindly made available to us by Roberto Terlevich and Jack Baldwin, which integrates the flux under the line profile and over a fitted linear or second order continuum. When more than one spectrum was available for a region in the same wavelength range, we used a S/N weighted mean. The main sources of error in line fluxes are different for CCD and IPCS spectra. We calculated the error for the IPCS line fluxes following Poisson photon statistics including sky and continuum. Additional errors coming from the exact location of the continuum were estimated to be negligible by consideration of repeated measurements.

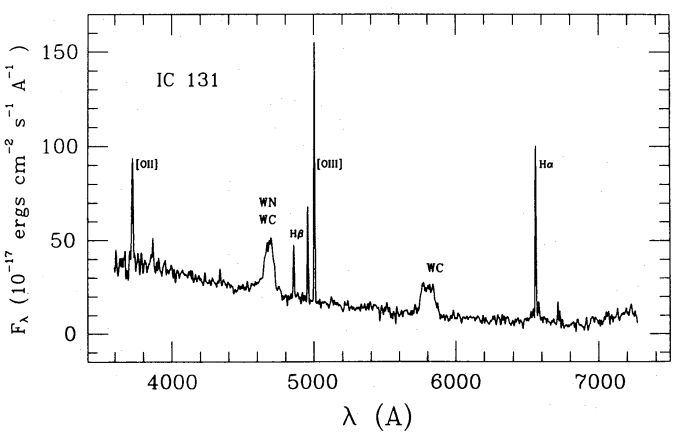

Figure 3. Intermediate dispersion IPCS spectrum of ICI 131. The underlying stellar population is conspicuous. Note the presence of the bands at $\lambda\lambda$4600 and 5850 Å characteristic of WC star(s), not previously noted in IC 131.

In the case of the CCD spectra, the calculated S/N ratio must include an additional noise contribution due to the readout noise of the chip, in our case $\sim 12\,e^{-}\text{pixel}^{-1}$ rms. However, in this case, the most important contribution to the error comes from the location of the continuum and the process of correction for atmospheric absorption. We estimated the error for these fluxes by means of repeated measurements and taking into account the standard deviation of the local continuum.

3.2 EXTINCTION

The reddening coefficient, $C(\mathrm{H}\beta)$, was determined using the observed quotients $\mathrm{H}\alpha/\mathrm{H}\beta$, $\mathrm{H}\gamma/\mathrm{H}\beta$, $\mathrm{H}\delta/\mathrm{H}\beta$ compared to the theoretical predictions for case B recombination (Brocklehurst 1971). The ratios were weighted by their corresponding baseline and S/N. Whenever the quality of the measurements allowed it, we have compared the ratio of Paschen lines to Hα with the prediction for case B recombination, obtaining generally acceptable agreement. The agreement is particularly good for NGC 595 which presents the highest quality CCD spectrum (Fig. 2c). Systematically, the values of $C(\mathrm{H}\beta)$ we found are similar to those given by Smith (1975) for the regions in common and lower than those obtained by Kwitter & Aller (1981).

The stellar continuum is very important in some cases; therefore some degree of absorption in the Balmer lines is expected due to the presence of early type stars. The effect of this absorption is to enhance the relative Balmer decrement going to the blue (see Paper I). This is particularly clear in NGC 604 and IC 131 where, using an iterative process, we found that a mean absorption equivalent width of 1.2 Å for Hα to Hγ provides an adequate correction. This value of EW(Hβ) is in good agreement with the findings of McCall *et al.* (1985), Skillman (1985) and Díaz (1988).

For NGC 595 and CC 93 we do not have enough information to derive an accurate value of the reddening coefficient, so we have adopted the determination of Smith (1975).

For the majority of the regions, the reddening appears to be very uniform, at least in the area of H II region enclosed by the slit, as can be seen in Fig. 4, where we present a direct comparison of

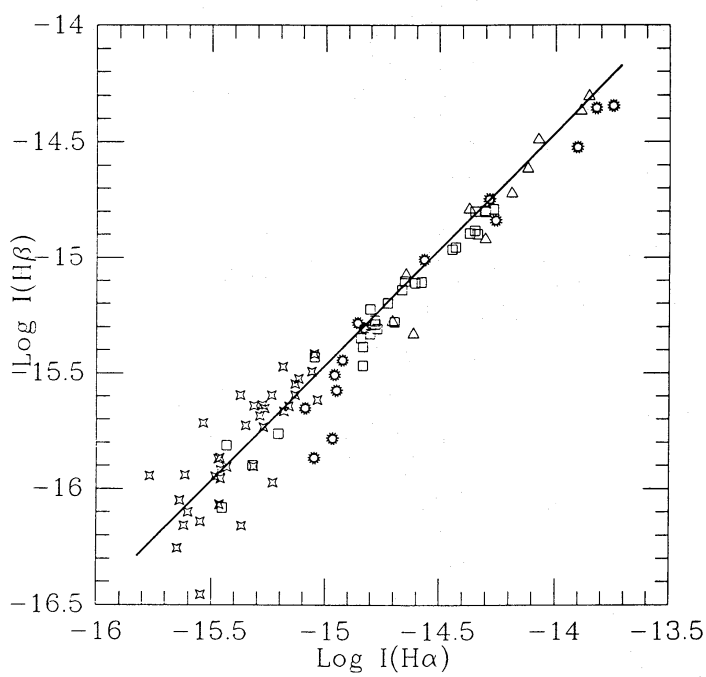

Figure 4. Comparison of the surface brightness (uncorrected for reddening) in Hα and Hβ along the slit for different H II regions: ✡ = IC 142; ¤ = IC 131; △ = MA 2; □ = NGC 588. The solid line corresponds to case B recombination.

Table 2. IPCS fluxes for the H II regions in M 33.

Region	$f(\lambda)$	CC 93*	IC 142	NGC 595	MA 2	NGC 604	IC 131	NGC 588
3727 [O II]	0.26	1738	2268±50	2138*	1837±50	2152±11	2090±30	1482±70
3750 H12	0.26					58±4		
3797 H10	0.26		18±5		13±3			
3835 H9	0.24		36±10		23±5			
3869 [Ne III]	0.23				93±13	108 ±2	472±75	415±30
3889 H8, He I	0.22		107±16		131±15	158±2		176±17
3969 [Ne III], Hε	0.21		137±11		144±17	175±2		205±17
4101 Hδ	0.18		221±12		214±19	250±2		262±18
4340 Hγ	0.135		487±13	450±3	460±20	443±4	410±60	500±19
4363 [O III]	0.13		<5(3σ)			7.5±1		24±5
4363 (H.R.)							21±4	31±3
4471 He I	0.10		16±3		38±8	37 ±4		30±5
4471 (H.R.)				29±2			34±7	32±5
4861 Hβ	0.00	1000	1000±16	1000±10	1000±30	1000 ±4	1000±70	1000±23
4959 [O III]	−0.02		258±11	466±20	583±24	775 ±7	1336±70	1662±30
5007 [O III]	−0.03	120	775±15	1430±40	1713±39	2077 ±8	3882±98	4647±45
5876 He I	−0.23		93±7		104±13	115 ±2		120±11
6300 [O I]	−0.30		3±1		15±4			
6548 [N II]	−0.34		193±11		83±13	124 ±2		33±7
6563 Hα	−0.34		2900±30		2763±50	2860 ±8	2630±98	2846±45
6584 [N II]	−0.34	324	646±18		272±23	335 ±4	305±50	97±10
6678 He I	−0.35		15±5		30±10	27 ±4		28±6
6717 [S II]	−0.36		260±20		125±2	166 ±4	274±60	111±12
6731 [S II]	−0.36	141	170±10		70±15	118 ±4	151±30	77±8
7065 He I	−0.40				10±4			
7135 [A III]	−0.41		34:		79:	55:		60:
7320 [O II]	−0.43				28±7			
F(Hβ)†			3.2		4.2	73.3	0.37	2.8
C(Hβ)		0.20*	0.24	0.49*	0.10	0.36	0.10	0.15
EW(Hβ) (Å)			117		107	86	20	97

*Smith (1975). †10^{-14} erg cm^{-2} s^{-1}.

uncorrected surface brightness in Hα and Hβ along the slit. Foreground galactic reddening can reach A_v=0.6 or C(Hβ)=0.3 (Humphreys 1980) and thus could account for most of the reddening that we find, but radio data show evidence for additional extinction (Viallefond & Goss 1986) which we neglect as it is effectively grey.

Reddening corrected line intensity ratios normalized to Hβ=1000 and 100 respectively are presented in Tables 2 and 3 for the IPCS and CCD observations. The flux in Hβ through each slit area and the reddening coefficient C(Hβ) are also given for each H II region, together with the equivalent width of Hβ.

3.3 PHYSICAL CONDITIONS: ELECTRON DENSITY AND TEMPERATURE

The physical conditions of the H II regions studied are listed in Table 4. Electron densities from the [S II]λλ6717,31 Å line ratio as in Paper I are consistent with the low density limit.

Electron temperatures are derived on the assumption of a two-zone scheme as in Paper I using variously auroral to nebular line ratios for [O III] for the high-ionization zone and [O II] and [S III] for the low ionization zone as available from our data or from the literature. In cases where temperatures are available for one zone only, we deduce that for the other from the approximate

Table 3. CCD fluxes for H II regions in M 33.

Region Line	$i(\lambda)$	$f(H\alpha)-f(\lambda)$	CC 93	IC 142	NGC 595	MA 2	NGC 604	NGC 588
6300 [O I]		−0.02			0.90±0.2			
6312 [S III]		−0.02			0.80±0.15			
6563 Hα	286	0.00	286±2	286±5.0	286±1.0	286±2.5	286.0±0.7	286±2
6584 [N II]		0.00	82.4±4.0	57.8±4.0	43.7±1.2	26.6±2	35.8±0.2	8.0±0.6
6678 [He I]		0.01		5.8±2.0	3.0±0.2	3.1±1	3.4±0.1	3.1±0.3
6717 [S II]		0.02	49±2.5	30.0±2.0	14.4±0.5	15.0±1.5	20.5±0.1	9.0±1.0
6731 [S II]		0.02	39±2.5	18.4±1.3	10.5±0.5	10.0±1.5	16.6±0.1	7.0±1.0
7065 [He I]		0.06			1.7±0.1	2.0±1	1.9±0.1	
7135 [A III]		0.07			8.1±0.6		9.2±0.4	10.0±1.0
7325 [O II]		0.09			2.7±0.3		3.4±0.2	
8665 P13	0.82	0.24			0.7±0.2			
8750 P12	1.11	0.25			1.0±0.1		1.4±0.3	
8863 P11	1.37	0.26			1.7±0.3		2.3±0.3	
9015 P10	1.85	0.28	1.2±0.6	3.9±2.0	1.6±0.2	1.9±0.8	2.7±0.3	
9069 [S III]		0.30	16.8±1.0	33.4±0.8	33.2±0.4	27.5±1	39.8±0.2	56.3±2
9229 P9	2.55	0.30	1.7±0.5	1.9±0.7	2.6±0.3	2.9±1	2.7±0.4	5.6±2
9532 [S III]		0.31	37.2±2.0	79.5±3.0	64.0±1.2	74±4	47.6±0.5	145.9±7.0
C(Hβ)			0.2*	0.24	0.49*	0.10	0.36	0.15

*Smith (1975).
$i(\lambda)$ are the expected values for the Paschen lines normalized to Hα=286 (case B, Brocklehurst 1971).

relationship predicted by photo-ionization models (Stasińska 1980a,b; 1982):

$$t[\mathrm{O\,II}]=t[\mathrm{O\,III}]-0.3(t[\mathrm{O\,III}]-1.0). \quad (1)$$

For the regions NGC 588 and 604 our derived temperatures are in good agreement with those given by Smith (1975); however, Kwitter & Aller (1981) find systematically larger values for t[O III], typically $\Delta t=0.2$, for NGC 588, 604 and IC 131, possibly because different slit positions were used. As will appear later, this difference could be very significant when calculating the global abundance gradient.

Table 4. Temperatures and densities for H II regions in M 33.

Region	CC 93	IC 142	NGC 595	MA 2	NGC 604	IC 131	NGC 588
t[O III]		≤0.9			0.77	0.95±0.06	1.01±0.03
t[O III]*		0.80	0.90	0.80	1.11	1.15	1.28
t[O III]†					0.90		1.00
t[O II]			0.85±0.07	0.90±0.07			
t[S III]			0.78±0.07				
$\langle t \rangle$	0.6	0.7	0.85	0.85	0.85	0.94	1.03
Log R_{23}	0.27	0.52	0.60	0.62	0.70	0.87	0.89
Adopted:							
$t(O^+)$	0.60	0.76	0.85	0.86	0.94	0.96	1.01
$t(O^{2+})$	0.55	0.69	0.80	0.80	0.77	0.95	1.01
x[S II]	0.02	0.00	0.01	0.00	0.00	0.00	0.03
x[S II]*		0.01	0.01	0.00	0.00	0.01	0.03

*Kwitter & Aller (1981).
†Smith (1975).

For CC 93 and IC 142, for which no auroral lines can be measured, we give average electron temperatures, $\langle t \rangle$, based on the empirical calibration of ([O II]+[O III])/Hβ, hereafter called R_{23}, as revised by Dopita & Evans (1986) and temperatures finally adopted for each zone using the procedure described below (Section 3.4).

3.4 IONIC AND TOTAL ABUNDANCES

Abundances of the most important ions have been calculated following the same algorithms as in Paper I, for a three level atom (McCall 1984) and the atomic data of Mendoza (1983); these are given in Table 5.

The estimated errors in the ionic abundances take into account the uncertainty in the derived temperature, the error in the line ratio used and the uncertainty in the reddening correction. In the case of IC 142 and CC 93 the adopted temperature is determined from theoretical models for which uncertainties are very difficult to quantify; therefore the contribution of the derived temperature to the total error in the abundances is not explicitly included. This could be important in the case of oxygen, but not in the case of sulphur or for abundance ratios such as N/O and Ne^{2+}/O^{2+}.

He^+/H^+ ratios are based on weighted means derived from $\lambda\lambda$4471, 5876 and 6678 Å lines using algorithms equivalent to those given by Kunth & Sargent (1983). Collisional excitation corrections, based on formulae given by Clegg (1987), are negligible and the observations of λ7065 Å give no evidence for significant fluorescence effects. In the case of IC 131 where only λ4471 Å is available, as a result of WC features, and the continuum is strong, we have added a correction of +15 per cent to allow for underlying stellar absorption assuming the equivalent width of the latter to be the same as estimated for NGC 5471 by Rayo, Peimbert & Torres-Peimbert (1982).

The conversion from ionic to total abundances used the ionization correction scheme presented in Paper I. The total He abundance has been computed as in Paper I, interpolating the ionization

Table 5. Ionic and total abundances for H II regions in M 33.

Region	CC 93	IC 142	NGC 595	MA 2	NGC 604	IC 131	NGC 588
12+log O^+/H^+	9.00±0.16	8.56±0.16	8.20	8.13	8.02±0.06	7.97	7.73±0.06
12+log O^{2+}/H^+	7.61±0.16	8.11±0.16	8.06	8.15	8.34±0.02	8.22	8.21±0.05
12+log O/H	9.02±0.16	8.70±0.16	8.44±0.09	8.44±0.15	8.51±0.03	8.41±0.06	8.30±0.06
log O^+/N^+	1.09±0.1	1.11±0.1	1.11±0.06	1.20±0.08	1.16±0.04	1.16±0.11	1.53±0.07
12+log N/H	7.92	7.57	7.33	7.24	7.35	7.25	6.77
12+log S^+/H^+	6.97±0.04	6.34±0.05	5.92	5.93	5.87±0.05	6.01±0.13	5.65±0.06
12+log S^{2+}/H^+	6.89±0.06	6.93±0.05	6.80	6.72	6.91±0.03		6.83±0.04
12+log S/H	7.23±0.06	7.03±0.05	6.86±0.08	6.8±0.1	6.95±0.03		6.86±0.06
$He^+/H^+ \times 10^2$							
4471 L.R.				7.6±1.6	7.3±0.8		6.1±1.2
4471 H.R.			5.8±0.5		7.3±0.2	7.9±1.2*	6.5±1.2
5876		6.3±0.6		7.4±0.8	8.1±0.3		8.9±0.8
6678		8.1±2.8	7.0±0.5	7.2±1.1	6.2±1.0		7.3±1.0
Log η	1.31	1.02	1.03	0.82	0.70		0.66
ICF		>1.2	>1.2	1.13	1.11	1.08	1.08
$\langle He/H \rangle \times 10^2$		>8.6	>8.2	8.33	8.3	8.5	8.3
Y		>0.256	>0.247	0.250	0.248	0.254	0.249
12+log O^{2+}/Ne^{2+}				0.74±0.1	0.78±0.02	0.45±0.09	0.61±0.08
12+log O^{2+}/Ar^{2+}		1.76	1.88	1.98	2.09	2.35	2.36

*15 per cent absorption correction following Rayo *et al.* (1982).

Table 6. H II region parameters in M 33.

Region	ϱ/ϱ_0	$T_{\rm eff}(*10^4{\rm K})$	log $(\bar{U}*c)$	log η
CC 93	0.03	3.40	6.91	1.31
IC 142	0.24	3.50	7.71	1.02
MA 2	0.30	3.50	7.94	0.82
NGC 595	0.42	3.50	7.97	1.03
NGC 604	0.60	3.70	8.09	0.70
IC 131	0.73			
NGC 588	0.96	3.75	8.17	0.66

ϱ_0=28′ (de Vaucouleurs, de Vaucouleurs & Corwin 1976).
i=54°.
Ω=22° (Warner, Wright & Baldwin 1973).

correction factor (ICF) from Stasińska models according to its relationship with the softness parameter η (Vílchez & Pagel 1988). For two regions, IC 142 and NGC 595, where the value of η implies an imprecision in the ICF, we give only a lower limit for the He abundance.

For the regions CC 93 and IC 142, for which we do not have direct information about electron temperature, we have derived the oxygen abundance in an independent way, i.e. by a combination of photo-ionization models (Stasińska 1980a) and two empirical parameters: R_{23} and $(O^+/O^{2+})(S^{2+}/S^+)$ (η; Paper I). A unique model from a grid can be selected once both empirical parameters are determined (Vílchez & Pagel 1988). The application of this method to CC 93 and IC 142 provides oxygen abundances in Table 5 and electron temperatures in Table 4, while the corresponding stellar effective temperatures and ionization parameters are given in Table 6.

4 Discussion

4.1 IONIZATION AND SEQUENCING PARAMETERS

It was suggested in our work on NGC 604 that the quotients R_{23}, [N II]/[O II], ([O II]/Hβ)(O II]/[S II]) and [N II]/[S II], are sufficiently constant within the same H II region that they could be potential abundance indicators.

The behaviour of [N II]/[O II] with respect to R_{23} has been discussed by McCall *et al.* (1985) and our pixel data are presented in Fig. 5. The ratio shows a general decrease with R_{23} changing over almost an order of magnitude for a 0.6 dex change in R_{23}. There is some scatter within each region, which is mainly accounted for by the observational errors.

The composite ratio ([O II]/Hβ)([O II]/[S II] was suggested by Evans & Dopita (1985) as an oxygen abundance indicator. This ratio was found to be constant over NGC 604, but we find it to be almost equally constant over the whole galaxy (Fig. 6), since for a total observed change of 0.6 dex in R_{23} (or 0.7 in log O/H) all the regions present the same value for the composite ratio, 1.5±0.15 dex. Therefore we find no significant advantage in using this ratio.

An interesting composite line ratio defined by Evans & Dopita (1985) is $\lambda\lambda$(6731/6563)(6731/9069), which they consider the best indicator of the ionization parameter, $\bar{U}$, although the absence of data for [S III] lines in most of the previous work led them to use [S II]/Hα as the ionization parameter indicator. The ionizing spectra in GEHR tend to be harder at lower abundances (Shields & Tinsley 1976; Stasińska 1980a; Campbell, Terlevich & Melnick 1986; Vílchez & Pagel 1988) and it has recently been found that $\bar{U}$ increases in the same sense (Evans & Dopita 1985; Dopita & Evans 1986; Evans 1986). Evans & Dopita (1985) predict that, for regions with oxygen abundances between 0.5 and 1 times solar, ionized by a representative

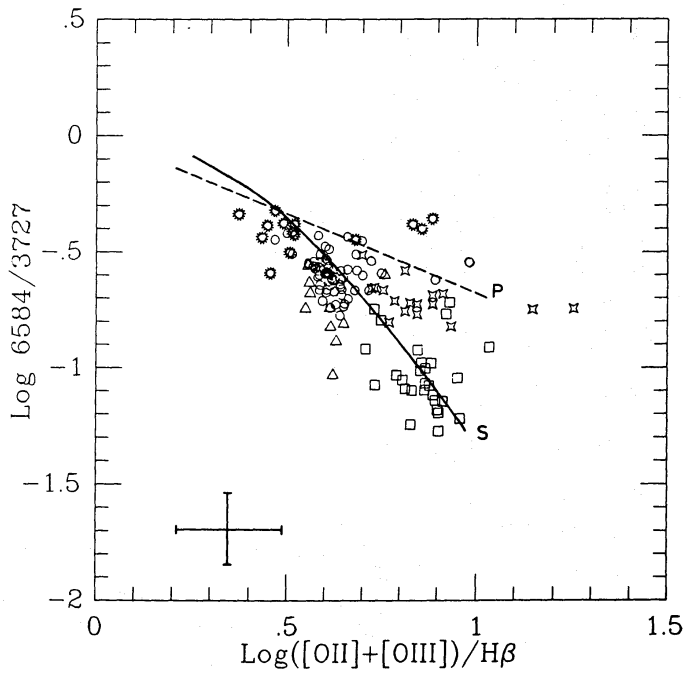

Figure 5. The behaviour of the logarithmic line intensity ratio [N II]/[O II] with respect to R_{23} (log ([O II]+[O III])/Hβ). Symbols are as in Fig. 4. 'Primary' and 'secondary' loci predicted by McCall *et al.* (1985) are shown for comparison. The three points from IC 142 with anomalously large ([O II]+[O III])/Hβ are affected by underlying absorption in Hβ.

star with effective temperature 4×10^4 K (unblanketed LTE models), an order of magnitude increase in $\bar{U}$ corresponds to a decrease by a factor of about 30 in this composite ratio.

We have computed $\bar{U}$ for the H II regions in M 33 by comparing the observed S^+/S^{2+} ratio with the predictions from Stasińska models with the same effective temperature [i.e. the same value of $\eta=(O^+/O^{2+})(S^{2+}/S^+)$] and the numbers are given in Table 6, defining $\bar{U}$ as the dimensionless ionization parameter at the edge of the Strömgren sphere which differs from the definition of Evans & Dopita (1985) by a constant factor of $(1/4c)$. In Fig. 7 we plot our values of $\bar{U}$against oxygen abundance showing also the values of the composite line ratio and Evans' values of $\bar{U}$ in M 101. There is amazingly good agreement despite the use of different stellar atmosphere models, different photo-ionization codes and different criteria on different objects, and the composite line ratio has an excellent correlation with $\bar{U}$ just as Evans & Dopita (1985) predicted. While it is too early to judge the precise mechanism governing the dependence of $\bar{U}$ on such parameters as chemical composition, dust content, initial mass function and age, it appears that model sequences assuming a constant value of $\bar{U}$ (McCall *et al.* 1985; Shields 1986) are excluded.

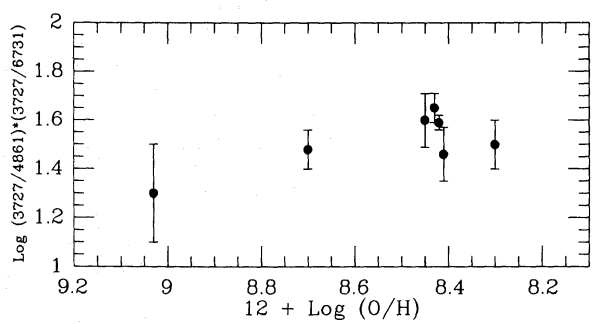

Figure 6. The composite ratio log([O II]/Hβ)×([O II]/[S II]) as a function of oxygen abundance. This ratio is practically constant over the disc of M 33 and thus cannot be used as an abundance indicator.

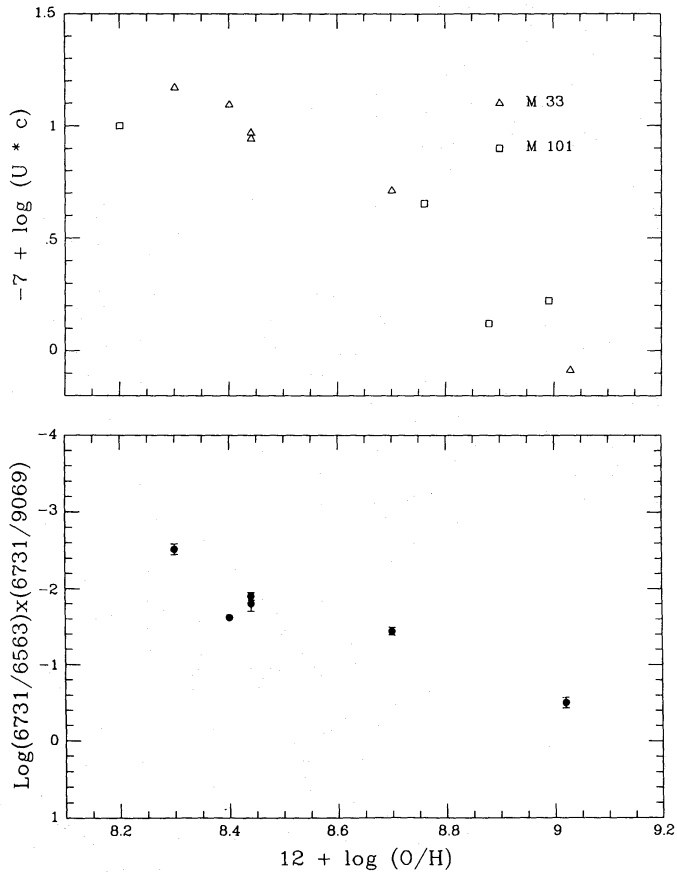

Figure 7. Upper panel: Ionization parameter from model fits in M33 (Table 6) and in M101 (Evans 1986). Lower panel: The composite ratio log([S II]/Hα×([S II]/[S III]) suggested by Evans & Dopita (1985) as an ionization parameter indicator, as a function of the oxygen abundance.

4.2 ABUNDANCE GRADIENTS

Helium

While the abundance ratios He^+/H^+ found in this work (Table 5) agree well with Smith (1975) and Kwitter & Aller (1981) for regions in common, the correction for the presence of neutral helium constitutes an important step in the determination of the gradient in the total He/H abundance.

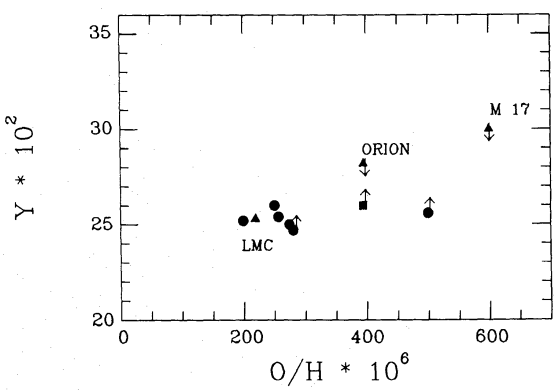

Figure 8. The He abundance by mass, Y, as a function of oxygen abundance for our observations in M33 (filled circles) and measures for the LMC and the Milky Way by Peimbert (1985) and Pankonin *et al.* (1980), taking account of the arguments of Cota & Ferland (1988).

In Fig. 8 we present helium abundances by mass, Y, versus oxygen abundance from our observations together with some measures for the Milky Way and LMC (Peimbert 1985; Pankonin, Walmsley & Thum 1980; Cota & Ferland 1988) and they are in good agreement with the relationship found for H II galaxies of low metallicity (Peimbert 1985; Pagel, Terlevich & Melnick 1986; Pagel 1988). However, the figure does not allow a clean determination of the helium gradient if any.

Oxygen

The existence of a gradient in the oxygen abundance is expected from the gradient in the electron temperature across M 33.

In Fig. 9 we present the O/H gradient determined from our abundance analysis. The most striking property of the gradient is that it seems to be steeper in the inner galaxy ($\varrho/\varrho_0<0.3$; see Table 6). For the outer region abundances ($\varrho/\varrho_0>0.3$) the logarithmic gradient can be fitted by $\Delta\log(O/H)/\Delta R=-0.06\pm0.01$ dex kpc^{-1} assuming a distance of 720 kpc (Allen 1973). For the overall gradient Kwitter & Aller find a value of -0.13 dex kpc^{-1}. Similarly, if we take into account all the points our overall gradient is $\Delta\log(O/H)/\Delta R=-0.12$.

The N/O gradient

Fig. 9 also shows the radial variation of nitrogen abundance in M 33 and in Fig. 10 we present the behaviour of log (N/O) versus the oxygen abundance. NGC 588, with an O/H abundance similar

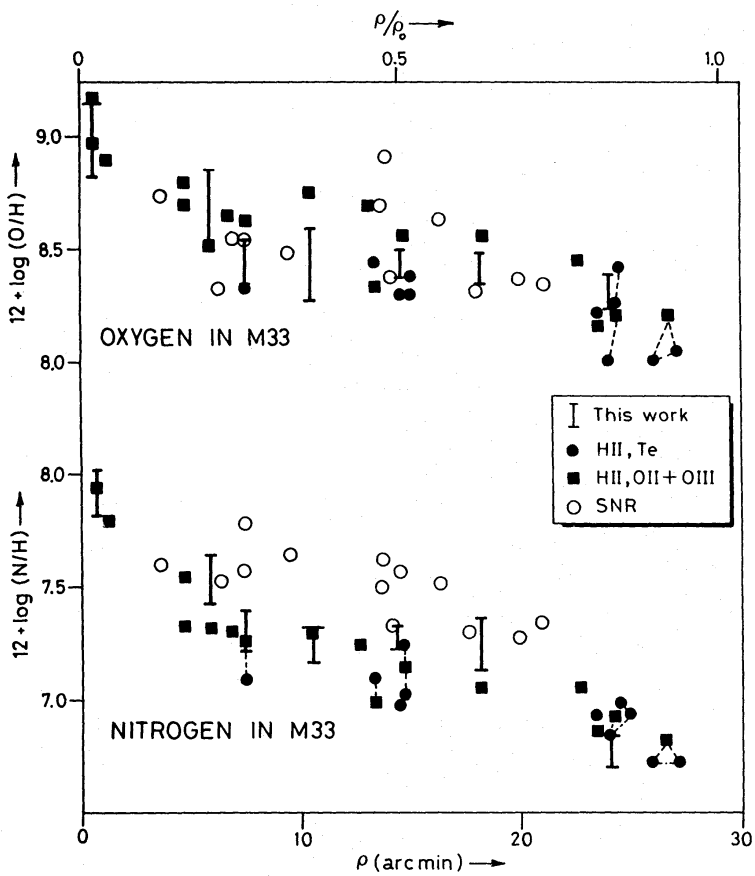

Figure 9. The radial oxygen and nitrogen abundance gradients in M 33 as deduced from H II regions and supernova remnants (Blair & Kirshner 1985). Data labelled H II, T_e and H II, O II+O III have been taken from observations by Smith (1975) and Kwitter & Aller (1981).

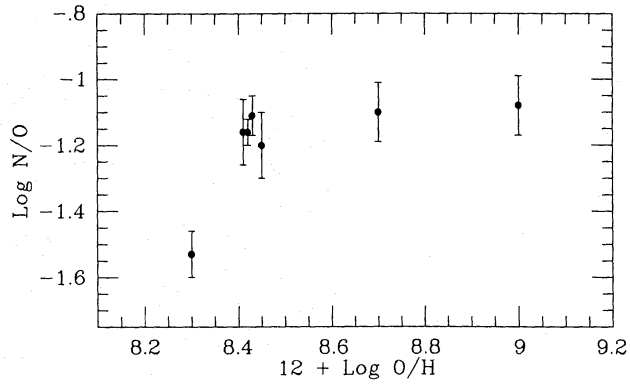

Figure 10. The N/O ratio versus the oxygen abundance for M33.

to the Large Magellanic Cloud, shows log N/O=−1.5 which is also similar whereas the other regions exhibit values similar to the Sun. Excluding NGC 588, there is a very small gradient $\Delta\log(N/O)/\Delta R = -0.03$ dex kpc^{-1}. The extrapolation of this slope to the distance of NGC 588 would give an N/O ratio larger than observed by a factor of 2.

In spiral galaxies it is not unusual to find a flat gradient of N/O and a strong one in O/H, with a mean N/O ratio increasing as a function of the mean metallicity (Pagel 1985). The N/O for irregular galaxies and low abundance objects in general remains almost constant (with some dispersion) around log (N/O)=−1.5, a similar value to the one we found for NGC 588. However, the SNR data and discrepancies between N^+/O^+ and infrared N^{2+}/O^{2+} ratios in our own Galaxy (Simpson *et al.* 1986; Lester *et al.* 1987; Rubin *et al.* 1988) leave a possibility that our N/O ratios at intermediate points in M 33 are too low.

Sulphur

It is now well known that the majority of the sulphur in most GEHRs is in the form S^{2+} (Shields & Searle 1978; Pagel 1978; Talent & Dufour 1979; Dennefeld & Stasińska 1983) whereas S^+ is an order of magnitude lower and the contribution due to S^{3+} and S^{4+} is not very important for the range of excitation conditions encountered in M 33 (Mathis 1982, 1985). Due to the lack of observation of the [S III] IR lines, the sulphur abundance has been poorly known so far, since the auroral [S III] line is very weak and difficult to measure. Our infrared observations allow the total S/H gradient to be derived and compared with the O/H gradient.

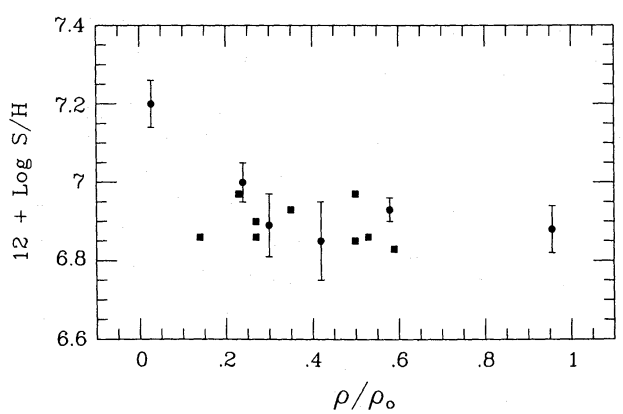

Figure 11. The radial sulphur abundance gradient in M 33. Solid dots represent data from this work. Filled squares are those by Blair & Kirshner (1985) from supernova remnants.

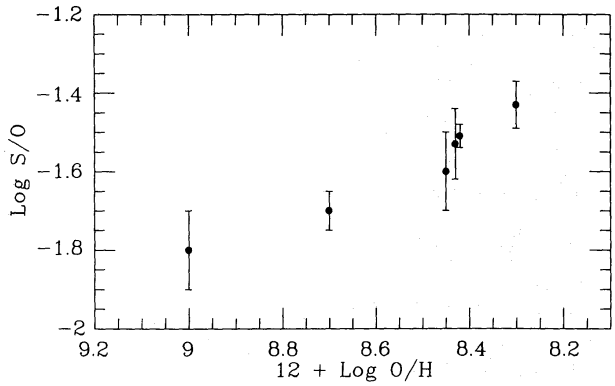

Figure 12. The S/O ratio as a function of the oxygen abundance in M33.

One can notice from Fig. 11 that the gradient of sulphur, although shallower, resembles that of oxygen over most of M 33. This result implies that the ratio of S/O shows a positive radial gradient over the disc of the galaxy. In Fig. 12 we present the ratio S/O versus the oxygen abundance. A least squares fitting gives a value $\Delta\log(S/O)/\Delta\log(O/H) = -0.51 \pm 0.02$, similar to the one found for M 101 by Evans (1986) using less direct methods.

The presence of a gradient in the S/O ratio is certainly a surprising result since it is normally assumed that both elements are primary and share a common origin. This gradient implies that the sulphur abundance diminishes more slowly with radius than O/H does, for a range in O/H abundance between 0.2 and 1.5 times solar.

Moreover, the S/H gradient we derive from the higher confidence supernova remnants in M 33 studied by Blair & Kirshner (1985) (Fig. 11) gives a similar value to the one deduced from our observations. Therefore there is a clear gradient of S/O in M 33 which undoubtedly has serious implications for nucleosynthesis and chemical evolution, as we will discuss later. A similar effect seems to be present in our Galaxy (Talent & Dufour 1979; Shaver *et al.* 1983) as well as in M 101 (Evans 1986) and it is no longer possible to dismiss it as an artefact.

4.3 ABUNDANCE GRADIENTS: IMPLICATIONS FOR NUCLEOSYNTHESIS

The abundance gradient in oxygen has been previously discussed by Pagel *et al.* (1978), Díaz & Tosi (1984), Edmunds & Pagel (1984) and Tosi & Díaz (1985). Considered from the point of view of the 'simple' closed model, all the oxygen abundances except that in CC 93 are compatible with a constant, low yield of about 0.003 by mass, whereas that of CC 93 suggests a yield of about twice this, whether this be due to mass inflow, mass outflow or variable initial mass function. The abundances are in accordance with the relation with disc surface density suggested by Edmunds & Pagel (1984).

The rather strange trend in N/O must be viewed with some caution because of the N^+/O^+–N^{2+}/O^{2+} discrepancy and the offset from the SNR results (Fig. 9). Nitrogen synthesis is believed to be predominantly due to stars near 2.5 $M_\odot$ (Maeder 1984) which burn carbon originally present or freshly synthesized and eject the products in planetary nebulae. In the first case, the nitrogen is a 'secondary' nucleosynthesis product for which the yield is expected in simple models to increase with the metallicity leading to an increase in N/O with O/H. In the second case it is a 'primary' product leading to constant N/O. These simple expectations, however, do not allow for effects of finite evolution time (which lead to trends in the ratio of all products from intermediate and low-mass stars relative to oxygen) and composition-dependent effects in stellar evolution which may enhance certain yields at low abundances. In addition, the ratio of primary to secondary yields

depends on the effectiveness of the third dredge-up process (which produces fresh carbon and primary nitrogen) and on the initial carbon abundance; also massive stars can produce secondary nitrogen in winds and secondary or primary nitrogen in interior processes, although their relative contribution is expected to be significant only at early times in galactic evolution because of their small numbers.

NGC 588, with a composition closely resembling that of the LMC, conforms to the pattern found in most irregular galaxies in which N/O has a constant ratio of about 0.035 (Pagel 1985, 1987). Infrared determinations of N^{2+}/O^{2+} in 30 Doradus confirm this value (Lester *et al.* 1987). This pattern is suggestive of mainly primary nitrogen production at low metallicities (Matteucci & Tosi 1985) whether in low or high mass stars; the behaviour of N/Fe in subdwarfs suggests the latter (Matteucci 1986).

The other H II regions in M 33 have a substantially larger value of N/O, although no smooth slope is evident. This could be taken as a sign of a contribution from secondary production or as a result of time-lag effects (*cf.* Edmunds & Pagel 1978) or changes in the initial mass function (Alloin *et al.* 1979) since determinations of C/N in H II regions from IUE data reveal no trend with metallicity up to solar (Pagel 1985).

Further evidence against a predominant effect of pure metallicity is provided by the large scatter of N/O as a function of O/H in spirals (Pagel 1985) and by the outermost H II region in M 81 which has LMC-like oxygen abundance but a solar-like N/O ratio (Garnett & Shields 1987).

Sulphur is a primary nucleosynthesis product and traditionally it is assumed that its production accompanied that of oxygen in a fixed proportion. This hypothesis is evidently not completely adequate since there is a gradient in S/O. Nevertheless, a systematic test of the S/O ratio in GEHRs has not been performed so far, mainly due to technical difficulties in the observation of [S III] far red lines and an additional lack of information about the exact ionization structure of sulphur in H II regions, which has led to incorrect abundances of S in the literature (see Pagel 1978; Barker 1980; Dennefeld & Stasińska 1983) before 1980 and even in some subsequent work. In order to investigate further the relationship between S/O and O/H abundances we have selected a collection of data from the literature in which S/H abundances are derived using [S III] and our (or an equivalent) ionization correction scheme (Fig. 13).

What is the reason for this variation in a ratio of primary elements? Evans (1986) suggests that

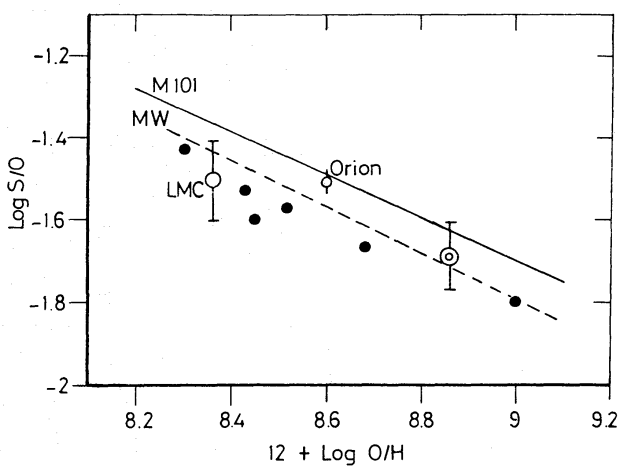

Figure 13. The S/O ratio as a function of oxygen abundance for M 33 (solid dots; this work); M 101 (solid line; Rayo *et al.* 1978; Shields & Searle 1978; Evans 1986); the Galaxy (broken line; Talent & Dufour 1979; Shaver *et al.* 1983; Dennefeld & Stasińska 1983). Data for the Sun, Orion and 30 Dor (Rosa & Mathis 1987) as well as the LMC (Dennefeld & Stasińska 1983) are also shown.

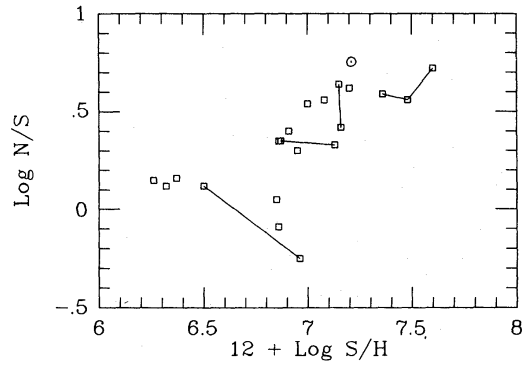

Figure 14. Relationship between the N/S abundance ratio and the sulphur abundance for the objects plotted in Fig. 13.

low and intermediate mass stars (IMS; $m<8\,M_{\odot}$) are formed in a higher proportion in the outer parts of a galaxy, and S production is enhanced (like Ar, Ca, Fe, C) due to enrichment from IMS and carbon deflagration supernovae. This hypothesis could explain the flatter S/H gradient. However, if N, S, and C come approximately from this range of masses, one would expect N/C and N/S to present a rather similar behaviour different from that observed in N/O. Fig. 14 shows the relationship between N/S and S/H for the selected sample of Table 7; here nitrogen seems to present an entirely 'secondary' relation with sulphur (*cf.* Evans 1986), in contrast with the constant N/C ratio.

In metal-deficient stars of the solar neighbourhood sulphur and oxygen show a broadly similar relationship with iron (François 1987) although, theoretically, some proportion of sulphur comes from carbon deflagration supernovae which also provide the majority of the iron in stars like the

Table 7. Selected sample of abundances.

Region	12+log O/H	log N/O	log S/O	Ref.
SMC	7.89	−1.48	−1.63	7
POX 4	7.93	−1.41	−1.56	6
NGC 5471	8.20	−1.49	−1.24	1
NGC 5471	8.19	−1.57	−1.69	2
NGC 588	8.30	−1.53	−1.44	3
30 Dor	8.37	−1.47	−1.52	4
NGC 604	8.51	−1.16	−1.56	8
NGC 595	8.44	−1.11	−1.53	3
MA 2	8.45	−1.24	−1.58	3
IC 142	8.70	−1.06	−1.60	3
Orion	8.62	−0.96	−1.53	4
NGC 5461	8.76	−1.30	−1.63	1
NGC 5461	8.62	−1.40	−1.75	2
Sun	8.88	−0.93	−1.69	4
H 40	8.99	−1.20	−1.84	1
H 40	8.81	−1.23	−1.65	2
CC 93	9.02	−1.09	−1.80	3
S 5	8.88	−0.93	−1.52	1
S 5	9.11	−0.79	−1.51	5

References: (1) Evans 1986; (2) Rayo *et al.* 1982; (3) This work; (4) Rosa & Mathis 1987; (5) Shields & Searle 1978; (6) Kunth & Sargent 1983; (7) Dennefeld & Stasinska 1983; (8) Díaz *et al.* 1987.

Sun (Isern *et al.* 1983; Thielemann, Nomoto & Yokoi 1986); sulphur might therefore be expected to show a trend intermediate between those of oxygen and iron. However, because of time-lag effects which account for the oxygen–iron 'anomaly' in nearby stars (Matteucci & Greggio 1986) even with a constant initial mass function, it cannot be taken for granted that the effects in young objects with different metallicities are identical to those found in local objects with different ages. Stars in the Magellanic Clouds, for instance, show no sign of the oxygen–iron effect found in nearby subdwarfs (Spite *et al.* 1986; Russell, Bessell & Dopita 1988) and it seems that even some 'reverse anomalies' can arise in numerical chemical evolution models (Matteucci, private communication).

5 Conclusions

We have consolidated and refined determination of the abundance trends in the H II regions of M 33, which were previously estimated on a less reliable basis in observation and interpretation of their spectra, by making spatially resolved observations and including the [S III] nebular lines in the far red. This has enabled us to give explicit values for the nominal effective temperatures of the ionizing star clusters and ionization parameters for the H II regions which show the same relationships with oxygen abundance as were found in M 101 by Evans (1986) using a somewhat different approach. Both the hardness of the ionizing spectrum and the ionization parameter increase at a substantial rate with diminishing abundance. We confirm previous indications that the oxygen abundance has a non-uniform spatial gradient, although closely related to mass density in the disc, and find trends in N/O and S/O for which the implications for nucleosynthesis and galactic evolution have yet to be explored. The striking agreement between oxygen and sulphur abundances derived for H II regions and supernova remnants at similar radial distances inspires confidence in both approaches to their determination, but there are discrepancies over nitrogen in M 33 as well as in our own Galaxy that remain to be clarified by further work. Nevertheless, the results of this paper provide a solid foundation for the determination of abundances in unresolved H II regions in more remote galaxies.

Acknowledgments

The INT is operated in the island of La Palma by the RGO at the Observatorio del Roque de los Muchachos of the Instituto de Astrofísica de Canarias. We specially thank I.R.G. Wilson for his support during the observations and the staff of the La Palma Operations Division for their help, and we thank both PATT and CAT for awarding observing time. We are also grateful for the warm hospitality of RGO and the IAC both during the realization of this work and the writing of the paper, and to E. D. Skillman for helpful comments thereon.

References

Allen, C. W., 1973. *Astrophysical Quantities*, 3rd edn, p. 287, Athlone Press, London.
Alloin, D., Collin-Souffrin, S., Joly, M. & Vigroux, L., 1979. *Astr. Astrophys.*, **78,** 200.
Barker, T., 1980. *Astrophys. J.*, **240,** 99.
Blair, W. P. & Kirshner, R. P., 1985. *Astrophys. J.*, **289,** 582.
Boulesteix, J., Courtes, G., Laval, A., Monnet, G. & Petit, H., 1974. *Astr. Astrophys.*, **37,** 33.
Brocklehurst, M., 1971. *Mon. Not. R. astr. Soc.*, **153,** 471.
Campbell, A. W., Terlevich, R. & Melnick, J., 1986. *Mon. Not. R. astr. Soc.*, **223,** 811.
Clegg, R. E. S., 1987. *Mon. Not. R. astr. Soc.*, **229,** 31P.
Cota, S. A. & Ferland, G., 1988, *Astrophys. J.*, **326,** 889.
Courtès, G., Petit, H., Sivan, J.-P., Dodonov, S. & Petit, M., 1987, *Astr. Astrophys.*, **174,** 28.
Dennefeld, M & Stasińska, G., 1983. *Astr. Astrophys.*, **118,** 234.

de Vaucouleurs, G., de Vaucouleurs, A. & Corwin, H. G., Jr., 1976. *Second Reference Catalogue of Bright Galaxies*, Texas University Press, Austin, TX.
Díaz, A. I., 1988. *Mon. Not. R. astr. Soc.*, **231**, 57.
Díaz, A. I. & Tosi, M., 1984. *Mon. Not. R. astr. Soc.*, **208**, 365.
Díaz, A. I., Terlevich, E., Pagel, B. E. J., Vílchez, J. M. & Edmunds, M. G., 1987. *Mon. Not. R. astr. Soc.*, **226**, 19.
Dinerstein, H. L. & Shields, G. A., 1986. *Astrophys. J.*, **311**, 45.
D'Odorico, S., Rosa, M. & Wampler, E. J., 1983. *Astr. Astrophys. Suppl.*, **53**, 97.
Dopita, M. A. & Evans, I. N., 1986. *Astrophys. J.*, **307**, 431.
Dopita, M. A., D'Odorico, S. & Benvenuti, P., 1980. *Astrophys. J.*, **236**, 628.
Edmunds, M. G. & Pagel, B. E. J., 1978. *Mon. Not. R. astr. Soc.*, **185**, 77P.
Edmunds, M. G. & Pagel, B. E. J., 1984. *Mon. Not. R. astr. Soc.*, **211**, 507.
Evans, I. N., 1986. *Astrophys. J.*, **309**, 544.
Evans, I. N. & Dopita, M. A., 1985. *Astrophys. J. Suppl.*, **58**, 125.
François, P., 1987. *Astr. Astrophys.*, **176**, 294.
Garnett, D. A. & Shields, G. A., 1987. *Astrophys. J.*, **317**, 82.
Humphries, R. M., 1980. *Astrophys. J.*, **241**, 587.
Isern, J., Labay, J., Hernanz, M. & Canal, R., 1983. *Astrophys. J.*, **273**, 320.
Kunth, D. & Sargent, W. L. W., 1983. *Astrophys. J.*, **273**, 81.
Kwitter, K. B. & Aller, L. H., 1981. *Mon. Not. R. astr. Soc.*, **195**, 939.
Lester, D. F., Dinerstein, H. L., Werner, M. W., Genzel, R. & Storey, J. W. V., 1987. *Astrophys. J.*, **320**, 573.
Maeder, A., 1984. *Stellar Nucleosynthesis*, p. 115, eds Chiosi, C. & Renzini, A., Reidel, Dordrecht, Holland.
Massey, P. & Conti, P. S., 1983. *Astrophys. J.*, **273**, 576.
Mathis, J. S., 1982. *Astrophys. J.*, **261**, 195.
Mathis, J. S., 1985. *Astrophys. J.*, **291**, 247.
Matteucci, F., 1986. *Publs astr. Soc. Pacif.*, **98**, 973.
Matteucci, F. & Greggio, L., 1986. *Astr. Astrophys.*, **154**, 279.
Matteucci, F. & Tosi, M., 1985. *Mon. Not. R. astr. Soc.*, **217**, 391.
McCall, M. L., 1984. *Mon. Not. R. astr. Soc.*, **208**, 253.
McCall, M. L., Rybski, P. M. & Shields, G. A., 1985. *Astrophys. J. Suppl.*, **57**, 1.
Mendoza, C., 1983. *Planetary Nebulae, IAU Symp. No.* 103, p. 143, ed. Flower, D. R., Reidel, Dordrecht, Holland.
Pagel, B. E. J., 1978. *Mon. Not. R. astr. Soc.*, **183**, 1P.
Pagel, B. E. J., 1985. *Production and Distribution of CNO Elements*, p. 155, eds Danziger, J., Matteucci, F. & Kjär, K., ESO, Garching.
Pagel, B. E. J., 1987. *Starbursts and Galaxy Evolution*, p. 227, eds Montmerle, T. & Van, J. T. T., Editions Frontieres, Paris.
Pagel, B. E. J., 1988. *ESO–CERN School on Astroparticle Physics*, p. 399, eds de Rujula, A., Nanopoulos, D., Shaver, P. A., World Scientific Singapore.
Pagel, B. E. J. & Edmunds, M. G., 1981. *Ann. Rev. Astr. Astrophys.*, **19**, 77.
Pagel, B. E. J., Edmunds, M. G., Fosbury, R. A. E. & Webster, B. L. 1978. *Mon. Not. R. astr. Soc.*, **184**, 569.
Pagel, B. E. J., Edmunds, M. G., Blackwell, D. E., Chun, M. S. & Smith, G., 1979. *Mon. Not. R. astr. Soc.*, **189**, 95.
Pagel, B. E. J., Terlevich, R. & Melnick, J., 1986. *Publs astr. Soc. Pacif.*, **98**, 1005.
Pankonin, V., Walmsley, C. M. & Thum, C., 1980. *Astr. Astrophys.*, **89**, 173.
Peimbert, M., 1985. *Star Forming Dwarf Galaxies and Related Objects*, p. 403, eds Kunth, D. & Thuan, T. X., Editions Frontieres, Paris.
Rayo, J. F., Peimbert, M. & Torres-Peimbert, S., 1982. *Astrophys. J.*, **255**, 1.
Rosa, M. & Mathis, J. S., 1987. *Astrophys. J.*, **317**, 163.
Rubin, R. H., Simpson, J. P., Erickson, F. & Haas, M. R., 1988. *Astrophys. J.*, **327**, 377.
Russell, S. C., Bessell, M. S. & Dopita, M. A., 1988. *Impact of Very High S/N Spectroscopy on Stellar Physics, IAU Symp. No 132*, p. 545, eds Cayrel de Strobel, G. & Spite, M., Reidel, Dordrecht, Holland.
Shaver, P. A., McGee, R. X., Danks, A. C. & Pottasch, S. R., 1983. *Mon. Not. R. astr. Soc.*, **204**, 53.
Shields, G. A., 1986. *Publs astr. Soc., Pacif.*, **98**, 1071.
Shields, G. A. & Searle, L., 1978. *Astrophys. J.*, **222**, 821.
Shields, G. A. & Tinsley, B. M., 1976, *Astrophys. J.*, **203**, 66.
Simpson, J. P., Rubin, R. H., Erickson, F. & Haas, M. R., 1986. *Astrophys. J.*, **311**, 895.
Skillman, E. D., 1985. *Astrophys. J.*, **290**, 449.
Smith, H. E., 1975. *Astrophys. J.*, **199**, 591.
Spite, M., Cayrel, R., François, F., Richtler, T. & Spite, F., 1986. *Astr. Astrophys.*, **168**, 197.
Stasińska, G., 1980a. *Astr. Astrophys.*, **84**, 320.

Stasińska, G., 1980b. *Astr. Astrophys.*, **85,** 359.
Stasińska, G., 1982. *Astr. Astrophys. Suppl.*, **48,** 299.
Talent, D. L. & Dufour, R. J., 1979. *Astrophys. J.*, **233,** 888.
Thielemann, F. K., Nomoto, K. & Yokoi, K., 1986. *Astr. Astrophys.*, **158,** 17.
Tosi, M. & Díaz, A. I., 1985. *Mon. Not. R. astr. Soc.*, **217,** 571.
Viallefond, F. & Goss, W. M., 1986. *Astr. Astrophys.*, **154,** 357.
Vílchez, J. M., 1987. *PhD thesis*, Universidad de La Laguna, Spain.
Vílchez, J. M. & Pagel, B. E. J., 1988. *Mon. Not. R. astr. Soc.*, **231,** 257.
Warner, P. J., Wright, M. C. H. & Baldwin, J. E., 1973. *Mon. Not. R. astr. Soc.*, **163,** 163.